Published online 8 December 2021 *Nucleic Acids Research, 2021, Vol. 49, No. 22* **13031–13044**
https://doi.org/10.1093/nar/gkab1178

Zippered G-quadruplex/hemin DNAzyme: exceptional catalyst for universal bioanalytical applications

Jia Li[1,2], Haiping Wu[2], Yurong Yan[2], Taixian Yuan[2], Yue Shu[1], Xin Gao[2], Lu Zhang[2], Siqiao Li[2], Shijia Ding[2,*] and Wei Cheng[1,*]

[1]The Center for Clinical Molecular Medical detection, The First Affiliated Hospital of Chongqing Medical University, Chongqing 400016, P.R. China and [2]Key Laboratory of Clinical Laboratory Diagnostics (Ministry of Education), College of Laboratory Medicine, Chongqing Medical University, Chongqing 400016, P.R. China

Received September 23, 2021; Revised November 09, 2021; Editorial Decision November 10, 2021; Accepted November 17, 2021

ABSTRACT

G-quadruplex (G4)/hemin DNAzyme is promising horseradish peroxidase (HRP)-mimic candidate in the biological field. However, its relatively unsatisfactory catalytic capacity limits the potential applications. Inspired by nature protease, we conducted a proximity-enhanced cofactor assembly strategy (PECA) to form an exceptional HRP mimic, namely zippered G4/hemin DNAzyme (Z-G4/H). The hybridization of short oligonucleotides induced proximity assembly of the DNA-grafted hemin (DGH) with the complementary G4 sequences (cG4s), mimicking the tight configuration of protease cofactor and apoenzyme. The detailed investigations of catalytic efficiency and mechanism verified the higher activity, more rapid catalytic rate and high environmental tolerance of the Z-G4/H than the classical G4/hemin DNAzymes (C-G4/H). Furthermore, a proximity recognition transducer has been developed based on the PECA for sensitive detection of gene rearrangement and imaging human epidermal growth factor receptor 2 protein (HER2) dimerization on cell surfaces. Our studies demonstrate the high efficiency of Z-G4/H and its universal application potential in clinical diagnostics and biomolecule interaction research. It also may offer significant opportunities and inspiration for the engineering of the protease-free mimic enzyme.

INTRODUCTION

G-quadruplex (G4) is a classical nucleic acid structure with stacked G-tetrads that assemble via Hoogsteen hydrogen bonding (1). When G4 specifically binds to hemin (Fe(III)-protoporphyrin IX), defined as a class of G4/hemin DNAzyme, the complex interestingly mimics horseradish peroxidase (HRP) catalytic properties (2,3). In such a DNAzymes complex, hemin is placed in the G4 binding pocket, woven together with the accessible G-quartets and surrounding nucleobases via π–π stacking (4). As a promising horseradish peroxidase (HRP)-mimic candidate, the DNAzyme complex possesses advantages of small size, facile synthesis and manipulation, being amenable to rational design through allosteric control, having a broad application potential in bioanalytical and biomedical fields and so on (5–8).

Although the advantages of G4/hemin DNAzymes are prominent, their relatively poor catalytic efficiency remains a significant challenge for practical applications. According to previous studies (9–11), to replicate the HRP peroxidase catalytic function, G4/hemin DNAzyme requires three major functional attributes: (I) a hydrophobic hemin-binding site, which is supplied by the G4 pocket; (II) guanine bases in a quartet arrangement, that serves as the proximal axial ligand of hemin, comparable to the histidine residue in HRP; (III) a distal ligand to undertake the function of general acid-base catalysis, an additional essential function of histidine in HRP. The above principles have guided efforts to improve the catalytic capability of the DNAzyme (12–15), although such improvements have not broken through the catalytic inefficiency bottleneck. Moreover, the ion-dependency of the G4 structure folding (such as K^+ or NH_4^+) or oxidative damage of guanine bases in the G-quartets could lead to environmental vulnerability and limited assembly efficiency in complex surroundings (16–18). Thus, establishing an excellent and robust DNAzyme that fulfills practical applications in complex environments is worthy of attention.

According to the principles mentioned above, the hexacoordinated hemin cofactor recruits the guanine bases of a G-quartet arrangement as its proximal axial ligand (similar to the histidine residue in HRP) to harvest the HRP-mimic catalytic ability (19–22). Hence, the activity status of hemin is crucial for the active center construct

*To whom correspondence should be addressed. Tel: +86 23 89011816; Fax: +86 23 68811487; Email: chengwei@hospital.cqmu.edu.cn
Correspondence may also be addressed to Shijia Ding. Email: dingshijia@163.com

and tuning of the G4/hemin DNAzyme. Several reports suggested that combining hemin with G4 via π–π stacking or covalent bonding with oligonucleotide chain would shift its dimerization/oligomerization equilibria towards monomeric (and catalytically active) form (23,24). Obviously, the monomeric state of hemin is more conducive to catalysis. In previous research (25,26), we reported an artificial oligonucleotide-grafted hemin DNAzyme without G4 sequence restraint, giving it unique advantages with solubility and programmability in protease-free assembly and programming that could potentially act as a flexible bioanalytic covalent bonding signal transducer.

The lack of hemin distal ligand that can act as a proton acceptor/donor of peroxide oxygen dragged down the catalytic capacity of such DNAzymes (9,27). Thus, adding an exogenous histidine mimic has been considered an effective supplement for promoting catalyzes, such as adenosine triphosphate (ATP) or spermidine (28,29). Furthermore, the modification of nucleobases (adenine (dA) or cytosine (dC)) in the flanking or loop sequence of G4 structure can also mimic an adjustable histidine reagent performing general acid-base catalysis and activate H_2O_2 prototropic cleavage in peroxidase catalysis, achieving enhanced catalytic performance (30–34). Such a regulation mechanism simulates the protease group replenishment and is a valuable inspiration for high-efficiency DNAzyme assembly.

Herein, we present a proximity-enhanced cofactor assembly strategy (PECA) based on the proximity assembly of the DNA-grafted hemin (DGH) with the complementary G4 sequences (cG4s) to form a zippered G4/hemin DNAzyme (Z-G4/H), which mimics the tight configuration of protease cofactor and apoenzyme. Following detailed investigations of the catalytic efficiency and mechanism of Z-G4/H, we developed a proximity recognition approach based on PECA for sensitive visual detection of gene rearrangement and imaging human epidermal growth factor receptor 2 (HER2) dimerization on cell surfaces. Briefly, we constructed the PECA strategy to provide powerful visual or imaging reporters for bioanalytical and diagnostic applications. It's also a profound inspiration for detailed understanding and elucidation of protease mimicry establishment.

MATERIALS AND METHODS

Materials and reagents

The sequences of DNA oligonucleotides used in the present study and the related abbreviations are listed in Supplementary Table S1. Unmodified DNA oligonucleotides were synthesized by Sangon Biotech (Shanghai) Co. Ltd. All modified, HPLC-purified oligonucleotides were obtained from Takara Biotechnology (Dalian, China). Their concentrations were determined by UV absorbance at 260 nm using the molar extinction coefficients provided by the OligoAnalyzer v3.1 tool (http://sg.idtdna.com/calc/analyzer). All oligonucleotides were dissolved in Tris-ethylene diamine tetraacetic acid buffer (pH 8.0, 10 mM Tris−HCl, 1 mM EDTA) and stored at −20°C. All other reagents were of analytical grade. All buffer solutions were prepared using Millipore-Q water (≥18 MΩ, Milli-Q, Millipore). Hemin was dissolved in dimethyl sulfoxide as a stock solution then diluted to the required concentration using 50 mM Tris−HCl buffer (pH 7.0, 25 mM KCl). To fold the G4 structure, DNA samples were heated to 95°C for 5 min, then cooled slowly to room temperature and stored at 4°C prior to use. Freshly prepared $ABTS^{2-}$ and luminol were dissolved in ultrapure water to a concentration of 4 mM before use. Except for the analysis of pH and K^+, all experiments were performed in 50 mM Tris−HCl (pH 7.0) containing 25 mM KCl. All the chemicals were obtained from Sigma.

Circular dichroism (CD) measurements

CD spectra were collected on a circular dichroism spectropolarimeter (Applied Photophysics) over the 220–350 nm wavelength range. All cG4s solutions (5 μM) were obtained by directly diluting DNA stock solutions with 50 mM Tris-HCl buffer containing 25 mM KCl (pH 7.0). The lamp was placed under a stable stream of dry purified nitrogen (99.99%) during experimentation. Measurements were repeated three times.

Measurement of DNAzyme activity

Annealed cG4s (100 nM) diluted from the corresponding stock solution were incubated with hemin (100 nM) or DGH (100 nM) in 50 mM Tris–HCl buffer for 30 min at 25°C. After the formation of the G4/hemin complexes, the $ABTS^{2-}$ (2 mM) or luminol (2 mM) and H_2O_2 (50 mM) were added, after which the products were analyzed by UV-vis spectroscopy over the range of 400–500 nm. Catalytic kinetics experiments were performed on an Agilent Cary100 spectrophotometer at 418 nm for 120 s. The initial rate (V_0, nM/s) of the oxidation reaction was calculated from the slope of the linear portion of increases of concentration of ABTS•- versus time (15 s). The concentration of ABTS•- was calculated based on the extinction coefficient of ABTS•- (36000 M^{-1}•cm^{-1}).All kinetic measurements were repeated three times.

The amount of G4/hemin DNAzyme molecule was measured by UV–vis absorption spectrophotometer in the wavelength range from 200 to 500 nm after the incubation of 1 μM free hemin, 1 μM C-G4/H, 1 μM DGH_5 probe, and 1 μM Z-G4/H at 25°C for 30 min, respectively.

Fluorescent quenching experiments of DNAzymes

The fluorescent quenching measurements were performed on the Cary Eclipse fluorescence spectrophotometer. FAM-labeled cG4s (1 μM) were incubated with hemin (1 μM) or DGH (1 μM) in 50 mM Tris–HCl buffer for 30 min at 25°C. After the incubation, 100 μl FAM-labelled cG4s, C-G4/H and Z-G4/H complex were moved to 1 mm quartz cuvette for the fluorescent spectra scan monitoring from 500 to 600 nm under the excitation at 485 nm. The silt widths of excitation and emission were both 5 nm and the voltage was 600 V.

Spectroscopic characterization of peroxidation intermediate

cG4s (1 μM) were incubated with hemin (1 μM) or DGH (1 μM) in 50 mM Tris–HCl buffer for 30 min at 25°C. H_2O_2

(2 mM) was added to evaluate the decay kinetics of the DNAzymes by recording the absorbance at 402 nm over time. To monitor the generation of Compound **I**, experiments were conducted in the presence of 5 μM cG4s, 5 μM hemin, 5 μM DGH, and 2 mM H_2O_2 in 50 mM Tris–HCl buffer. Spectra were collected over the range of 450 to 700 nm as a function of time.

DNAzymes activities under different conditions

cG4s (100 nM) were incubated with 100 nM hemin or DGH at 25°C for 30 min, after which 2 mM $ABTS^{2-}$ and 50 mM H_2O_2 were added to initiate the enzymatic reaction. Plots of absorbance at 418 nm versus reaction time of DNAzymes were collected using an Agilent Cary100 spectrophotometer. The activities of DNAzymes under different K^+ conditions were investigated in Tris–HCl buffer containing 0, 5, 10, 25, 50, 75, 100, 125, 150, 200 mM K^+, respectively. The activities of DNAzymes under different pH were evaluated in 20 mM Britton–Robinson buffer (pH 2.83–7.08). All buffers contained 20 mM acetic acid, 20 mM orthophosphoric acid, 20 mM boric acid, and 100 mM KCl. Data were converted to V_0 values as described above. All measurements were repeated three times.

The stability of DNAzymes under different temperatures was carried out in Tris–HCl buffer after incubating cG4s (100 nM) with 100 nM hemin or DGH at 4, 20, 37, 60, 95°C for 30 min, respectively. The concentration of HRP was 2 μg/ml. The UV-vis absorption peaks value of DNAzyme peroxidation product ABTS•- was analyzed by UV-vis spectroscopy over the range of 400–500 nm. The stability of DNAzymes in complex surroundings was measured in 0, 20, 50, 100, 200-fold dilution serum containing 25 mM KCl after incubating cG4s (100 nM) with 100 nM hemin or DGH at 25°C for 30 min. All measurements were repeated three times.

Analytical performance of Z-G4A/H for the detection of the BCR-ABL fusion gene and HER2 dimerization

To detect the BCR-ABL fusion gene, 1 μl target BCR-ABL fusion gene at various concentrations was added to a 98 μl reaction mixture containing 100 nM of cG4s, 100 nM hemin, or DGH probe, and incubated at 37°C for 30 min. A 100 μl aliquot of 4 mM $ABTS^{2-}$ and 1 μl of 10 M freshly prepared H_2O_2 were then added and reacted at room temperature. Finally, the absorbance spectra were recorded, as described above.

For HER2 dimer detection, the human breast cancer cell lines SKBR-3, MDA-MB-231 and MCF-7 were seeded on glass coverslips pretreated with TC in a 24 well plate and cultured in DMEM medium (10% fetal bovine serum, 1% penicillin, 1% streptomycin) at 37°C in a 5% CO_2 incubator. Then, the cells were fixed in 4% paraformaldehyde for 15 min at room temperature and washed three times using ice-cold PBS. The 3% H_2O_2 was used to inhibit the endogenous peroxidase activity for 30 min, and a blocking buffer containing 3% BSA and 0.4 mg/ml salmon sperm DNA in PBS was used to block nonspecific binding at 37°C for 1 h. The cell slides were then washed twice using ice-cold PBS until analyzed. To image HER2 protein identity on cell surfaces, a mixture of 400 μl 200 nM HER2-apt-G4 and 400 μl 200 nM hemin or HER2-DGH probes in Tris–HCl buffer were used for HER2 homodimer detection. After reacting with the corresponding probes at room temperature for 2 h, the cell slides were incubated with a tyramide reaction mixture containing Alexa Fluor™ 488 tyramide reagent (1:300) and 3% H_2O_2 at room temperature for 10 min in the dark. Cell nuclei were stained with DAPI solution for 5 min. After each step, the cells were washed three times in 0.05% Tween 20 in PBS for 5 min. Finally, the cells on the slides were analyzed by a fluorescence microscope using identical parameters for exposure. For flow cytometry, a suspension of 10^6 cells was incubated with the corresponding probes to form DNAzymes, which were then reacted with the tyramide reaction solution. The fluorescence intensity of the cells was then recorded by a FC-500 flow cytometer. The Alexa Fluor 488-tyramine catalytic substrate used in this method had the same excitation (495 nm) and emission (519 nm) wavelengths as fluorescein isothiocyanate (FITC), which enabled the FITC channel for general fluorescence microscopy to be used for the analysis of imaging.

RESULTS

Principle of the PECA

The relatively simple structure, fragile ion-dependent folding and π–π stacking mode of C-G4/H may lead to insufficient catalytic ability in the homogeneous environment (Figure 1A **I**). Inspired by the combine-activated manner of apoenzyme and cofactors in protease (35,36), we conducted a proximity-enhanced cofactor assembly (PECA) through hybridization of the complementary G4 sequences (cG4s) and DNA-grafted hemin (DGH) probes (Figure 1A **II**). Through complementary oligonucleotides hybridization, hemin was situated at the end of the duplex, adjacent to the G4 structure, and then achieved the assembly of Z-G4/H. For further significant improvement, we modified intramolecular adjacent nucleobases at the G4 core sequence as a distal ligand of hemin. Accordingly, an adjacent adenine modified Z-G4/H was presented as Z-G4A/H (Figure 1A **III**), part of the Z-G4/H-based DNAzymes (Z-G4/Hs). Z-G4/Hs could promote and accelerate H_2O_2 prototropic cleavage in peroxidase catalysis (30), such as oxidation of 2,2'-azino-bis(3-ethyl benzothiazole-6-sulfonic acid) ($ABTS^{2-}$) (Figure 1B), luminol and tyramine (37–39). The DGH probe was synthesized via an amide reaction. DGH_5 and DGH_3 were referred to as the covalent attachment of hemin to the 5' and 3'-terminal oligonucleotide chain, respectively (Supplementary Figure S1). Two classical G4 sequences, PS2.M (non parallel-type) and G3T (parallel-type) were employed to constitute cG4s (the abbreviations and sequences of cG4s were shown in Supplementary Table S1). The typical topologies of DNAzymes in the present study were characterized by circular dichroism (CD) (Supplementary Figure S2).

The catalytic activity of Z-G4/H

To evaluate the catalytic capability of Z-G4/H, UV–vis and chemiluminescence experiments were carried out via the catalysis of substrate $ABTS^{2-}$ and luminol with H_2O_2, respectively. The schematic diagram of the C-G4/H and

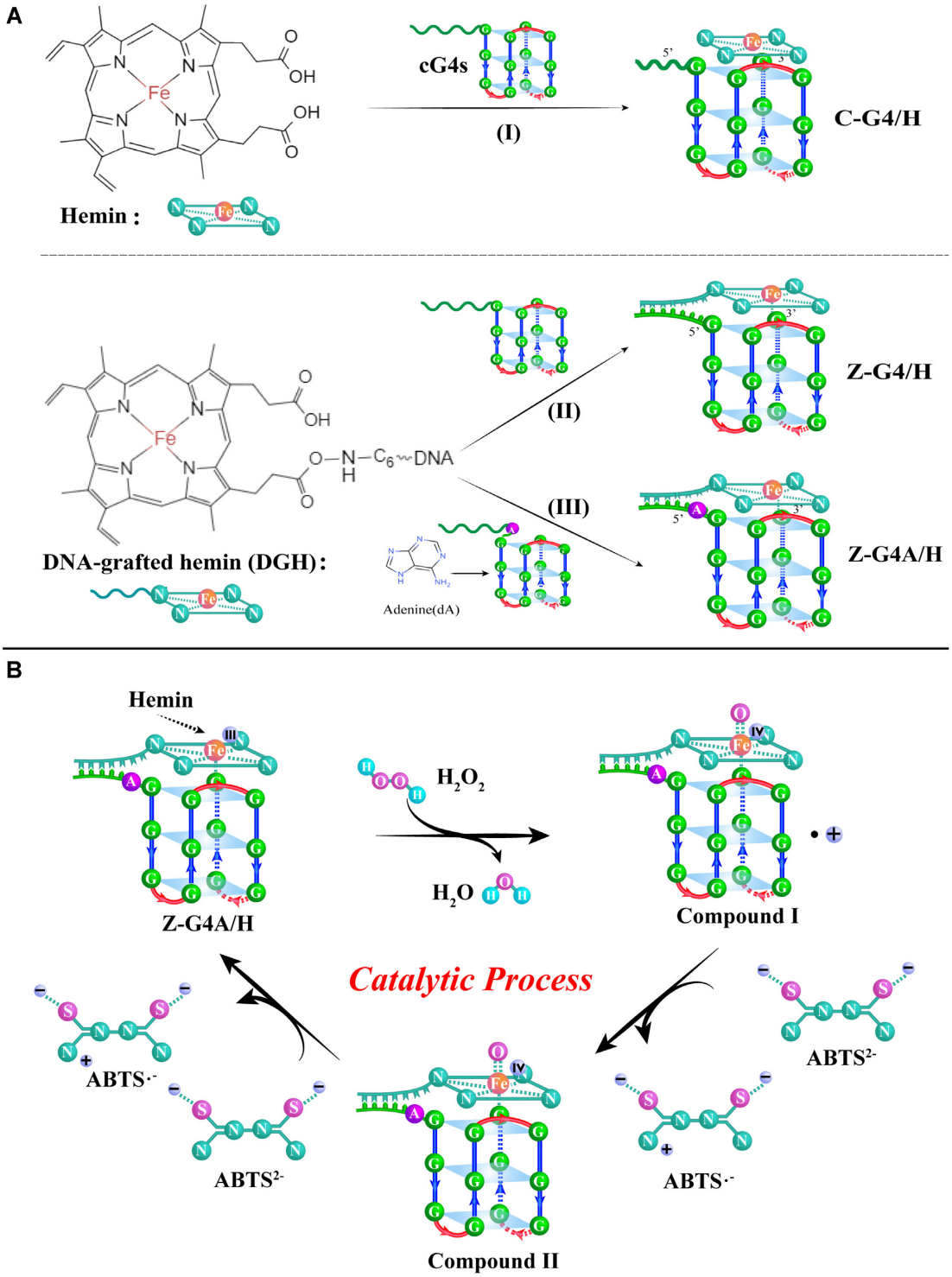

Figure 1. (A) Schematic representation of (**I**) C-G4/H, (**II**) Z-G4/H and (**III**) Z-G4A/H assembly. (B) The catalytic process of the Z-G4A/H catalyzes the substrate $ABTS^{2-}$ and H_2O_2.

Z-G4/H assembly structure (PS2.M-based) was presented in Figure 2A. As shown in Figure 2B, the UV-vis absorption spectra of the $ABTS^{2-}$–H_2O_2 system displayed absorption peaks at 418 nm, which oxidated from $ABTS^{2-}$ to a green-colored ABTS•- by DNAzymes. Surprisingly, the UV-vis absorption peak at 418 nm of Z-G4/H (curve f) displayed a 3-fold increase compared with the faint peak of C-G4/H (curve d), revealing a significant improvement of the DNAzyme activity owing to the effectiveness of PECA. Furthermore, an almost 11-fold greater absorption peak of Z-G4A/H (curve g) was observed than C-G4/H, demonstrating that the supplement of adjacent dA nucleobase in the hemin binding site resulted in excellent catalytic performance. By contrast, the dA supplement of C-G4/H brought very weak enhancement (curve e), further indicating the superiority of PECA and the importance of the catalytic active center architecture (31,34). In addition, the catalytic efficacy of Z-G4/H was also probed by UV-vis kinetics experiments (Figure 2C), and the corresponding catalytic initial rate (V_0, nM/s) results showed an approximately 12-fold increase of Z-G4A/H (948.89 nM/s) than that of C-G4/H (77.22 nM/s) (Figure 2D). Similarly, chemiluminescence experiments results were consistent with the UV-vis absorption and kinetics experiments, validating the enhanced catalysis of Z-G4/Hs (Figure 2E). Furthermore, we compared the activity of Z-G4A/H DNAzyme and HRP protein with an equal amount of hemin quantified by the absorption peak at 402 nm. (Supplementary Figure S3A). As shown in Supplementary Figures S3B-S3D, both the absorbance of products and kinetics results revealed that the PECA strategy shortens the gap between classical G4/hemin DNAzyme and protease by about 9 times, demonstrating the novel Z-G4/Hs possessed a catalytic capability substantially greater than that of the C-G4/Hs, even had a chance to be comparable to protease.

For a detailed exploration of the effectiveness of PECA, we characterized the amount of the assembled G4/hemin molecule of Z-G4/H by UV-vis absorption spectrophotometer at 402 nm. As shown in Supplementary Figure S4A, a higher G4/hemin DNAzyme characteristic absorption peak of Z-G4/H (curve d) at 402 nm was observed than C-G4/H (curve c), illustrating more G4/hemin DNAzyme molecules assembly in Z-G4/H. Besides, we found that the signal peaks increased with an increasing number of complementary nucleobases from 0, 6, 12, 18 to 24 in the Z-G4/H (Supplementary Figure S4B), indicating increased complementation lead to enhanced catalytic ability. These results suggested the high assembly efficiency and proximity complementation effect of PECA design brought about an overwhelming enhancement activity, resulting in a well-executed catalytic system.

Activity analysis of Z-G4/H variants

To further understand the catalytic capacity and mechanism of Z-G4/H, we assembled a series of Z-G4/H variants and then measured the UV-vis absorption peaks value of DNAzyme peroxidation product ABTS•- at 418 nm. Firstly, the parallel-type Z-G4/H was analyzed to probe the influence of G4 topology on catalytic capability (Figure 3A a group). As shown in Figure 3B, slight catalytic enhancements of the parallel-type Z-G4/H (a0–a3) were observed than the non-parallel-type (bA0–bA3), indicating a weak catalytic effect of G4 topology in Z-G4/H. Previous studies reported that the role of dA was particularly significant in parallel-type C-G4/H (23). However, our data indicated that both parallel and non-parallel Z-G4A/H DNAzymes exhibited exceptional catalytic capacity, confirming the greater catalytic activity influence of the dA modification than that of topology.

To elucidate the specific effect of nucleobases modification at the active catalytic site, a series of Z-G4/H variants were formed through the assembly of the different numbers and types of nucleobases modified cG4s with DGH_5 (Figure 3A b group). As shown in Fig 3B, the catalytic activity of Z-G4/H was related to the type of nucleobase modification, either dA (bA1–A3) or dC (bC1–C3), boosted the catalytic ability. Instead, the dT hadn't had such a similar promoting effect (bT1–T3). These results are consistent with the previous studies that adenine and cytosine were proved to mimic the distal histidine residue of the peroxidase enzyme, activating H_2O_2 for facilitating its transfer to the hemin iron atom accelerate the compound I formation in the catalytic cycle but thymine unable to assist this transfer (28,32,33). Thus, the dA or dC could both improve the G4/hemin-based DNAzyme activity. Though, the activity of Z-G4/H increased more observably with the increased number of dCs than dAs, because the increased number of dA with a larger purine ring would lead to more steric effects. The activity enhancement of the dA was indeed stronger than dC. A single dA even was comparable to three dCs. It was due to richer electrons of dA than dC (31). These results demonstrated that certain nucleobases close to the G-quartet boosted peroxidation activity resulting in enhanced DNAzyme activity. Furthermore, compared with the catalytic ability of intramolecular nucleobases-modified G4 DNAzymes in previous reports (31), a nearly 3.7-fold increase of Z-G4A/H was observed than the formers (Supplementary Figure S5). Hence, we suspected that the dA or dC residue act as an effective distal ligand supplement of hemin in PECA design, constituting a more HRP-like aggregation of the active catalytic site and contributing to the boost of catalytic activity.

We were also curious about the influence of the nucleobases modification manner in DGH. When cG4s assembled with different nucleobases modified DGH_5 (Figure 3A c group), the results indicated its similar enhancement effect of the cG4s nucleobases modified manner. However, the improvement did not match the latter's (Figure 3B c1–c3). Besides, we found no double enhancement resulting from the direct assembly of the nucleobases modified DGH with the dA modified G4 sequence, implying a non-optimal binding site or the finiteness of spatial location in the active site lead to unexpected enhancement. The stacking mode and location of hemin in the G4 catalytic binding site play an important role in DNAzymes (33,35). To verify the stacking influence of hemin in Z-G4/H, we fine-tuned the stacking mode by modification at the 3' end of DGH, hybridizing with the cG4s (Figure 3A e group). As displayed in Figure 3B

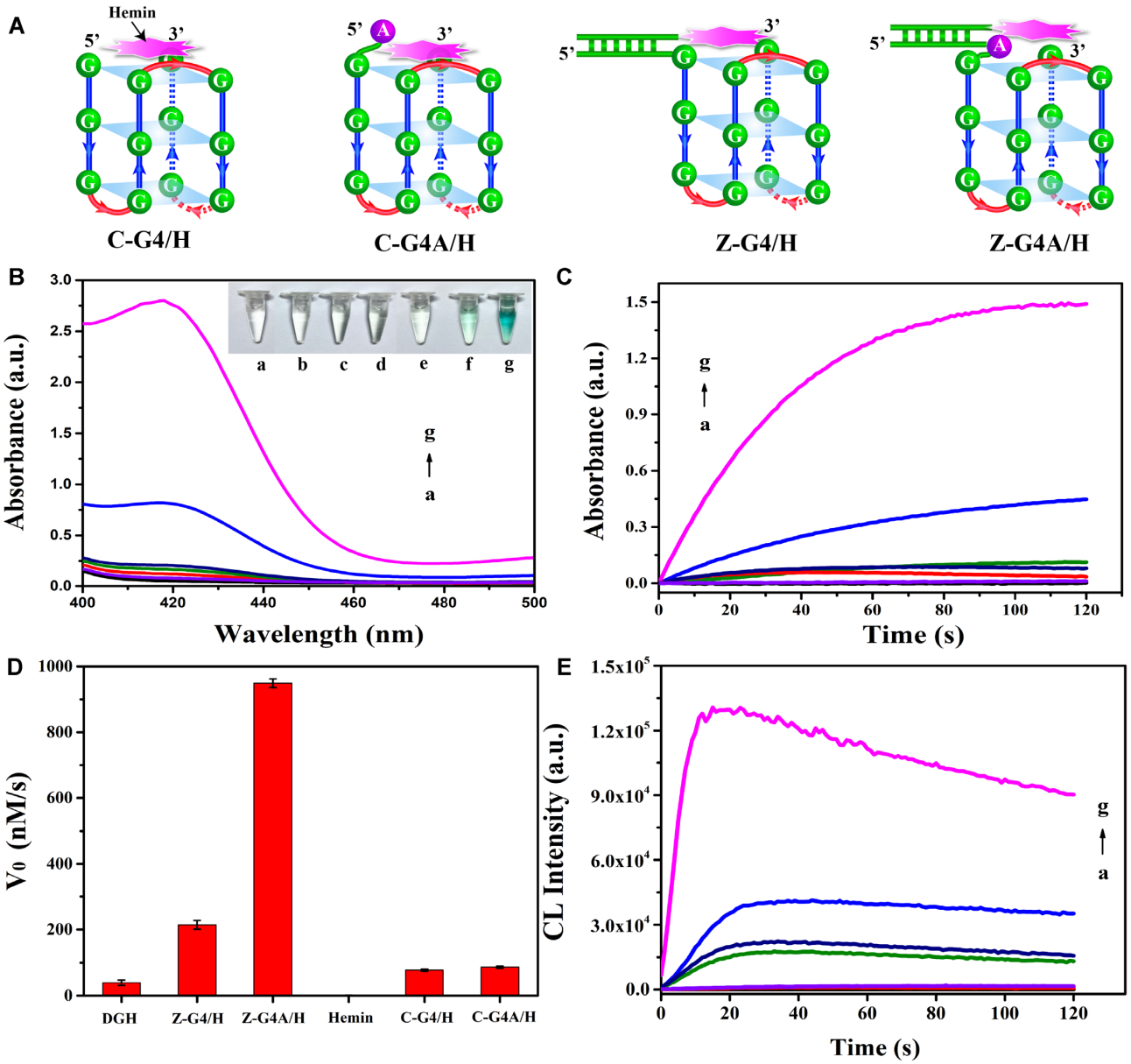

Figure 2. (**A**) Schematic representations of DNAzymes assembly structure. (**B**) Absorbance spectra of (a) blank, (b) 100 nM hemin, (c) 100 nM DGH_5, (d) 100 nM C-G4/H, (e) 100 nM C-G4A/H, (f) 100 nM Z-G4/H and (g) 100 nM Z-G4A/H after incubation with 2 mM $ABTS^{2-}$ and 50 mM H_2O_2. (**C**) Absorbance kinetic curves and (**D**) DNAzyme activity (V_0, expressed as nM/s) of (a)–(g) after incubation with 2 mM $ABTS^{2-}$ and 50 mM H_2O_2. (**E**) Chemiluminescence analysis of (a)–(g) in the presence of 2.0 mM luminol and 50 mM H_2O_2. Error bars represent standard deviations of three independent experiments.

e1–e3, the catalytic activity of DGH_5-based Z-G4/H showed almost double that of DGH_5-based DNAzymes, implying different stacking sites of hemin resulting in catalytic activity discrepancy.

To further elucidate the stacking mechanism, fluorescent quenching experiments were conducted using FAM-tagged G4 to monitor hemin-stacking. Hemin could quench the proximate fluoresce via electron transfer (30). As the negligible catalytic effect of G4 topology in Z-G4/H, we employed the parallel type structure (G3T) as a model to study the stacking mechanism of hemin. The FAM fluorophore was labeled at the 5'-end, on loop1, loop2 or loop3, or at the 3'-end of the G4 sequence, respectively (Figure 4A). As shown in Figure 4B, the fluorescence intensity of all Z-G4/H DNAzymes (blue column) was largely quenched than C-G4/H (red column), verifying the closer hemin binding and tight configuration of the Z-G4/H. In addition, the results suggested that the intensity of FAM fluorophore attached at the 3'-end in both two type DNAzymes decreased more than the others label sites, indicating the preference for hemin stacking at the 3'-end. It was also consistent with the known knowledge that hemin in these DNAzyme complexes is end-stacked upon rather than intercalated into G-quadruplex (11).

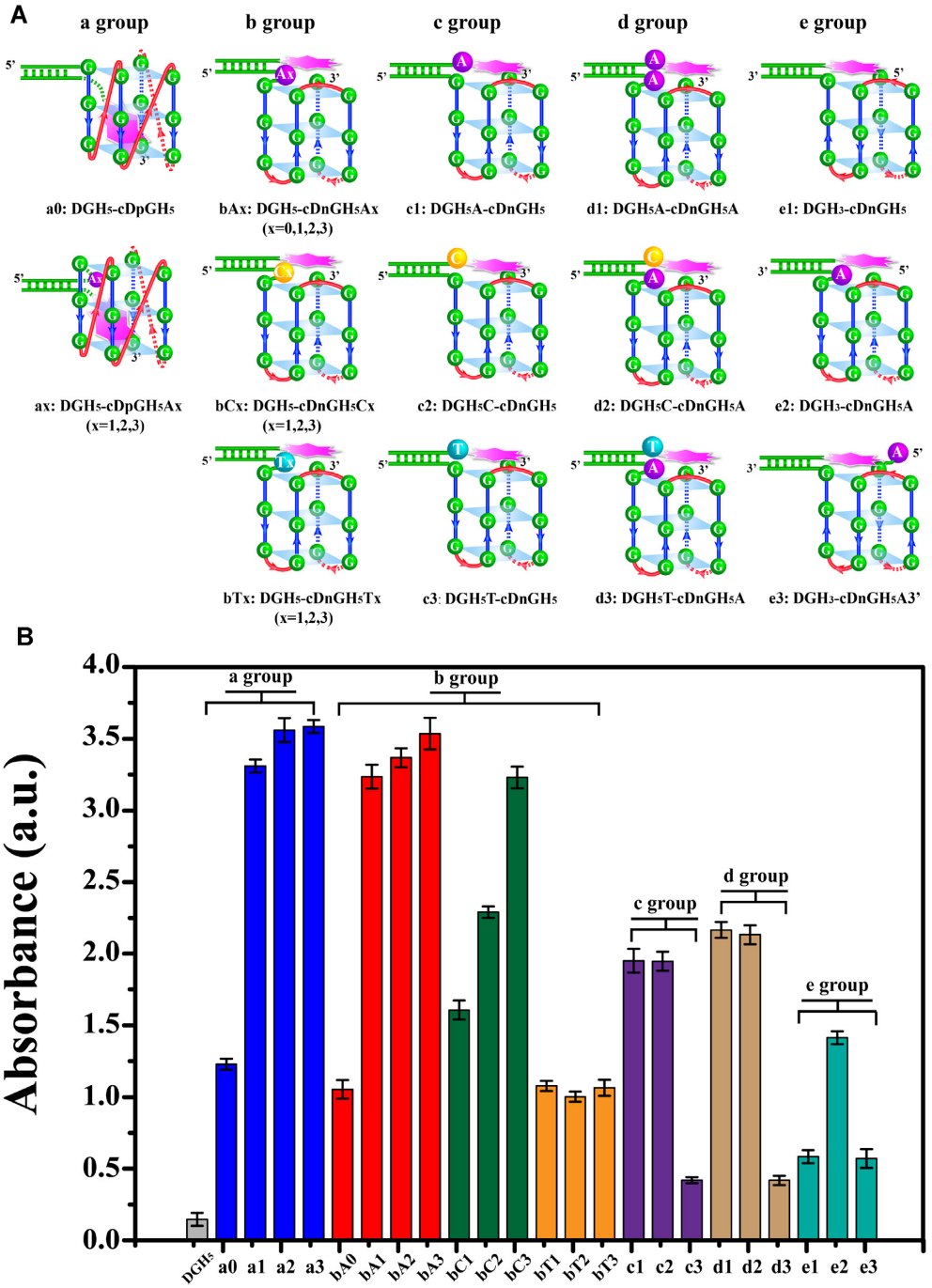

Figure 3. (**A**) Schematic representations of the Z-G4/H variants for activity analysis. (a group) represents the non or different nucleobases modified parallel-type cG4s assembled with DGH_5; (b group) represents non or different nucleobases modified non-parallel-type cG4s assembled with DGH_5; (c group) represents cG4s assembled with different nucleobases modified DGH_5; (d group) represents dA modified cG4s assembled with different nucleobases modified DGH_5; (e group) represents non-parallel-type cG4s assembled with DGH_3. (**B**) The absorbance of peaks of Z-G4/H variants DNAzymes after incubation with 2 mM $ABTS^{2-}$ and 50 mM H_2O_2. X represents the number of modified nucleobases. Error bars represent the standard deviation of three independent experiments.

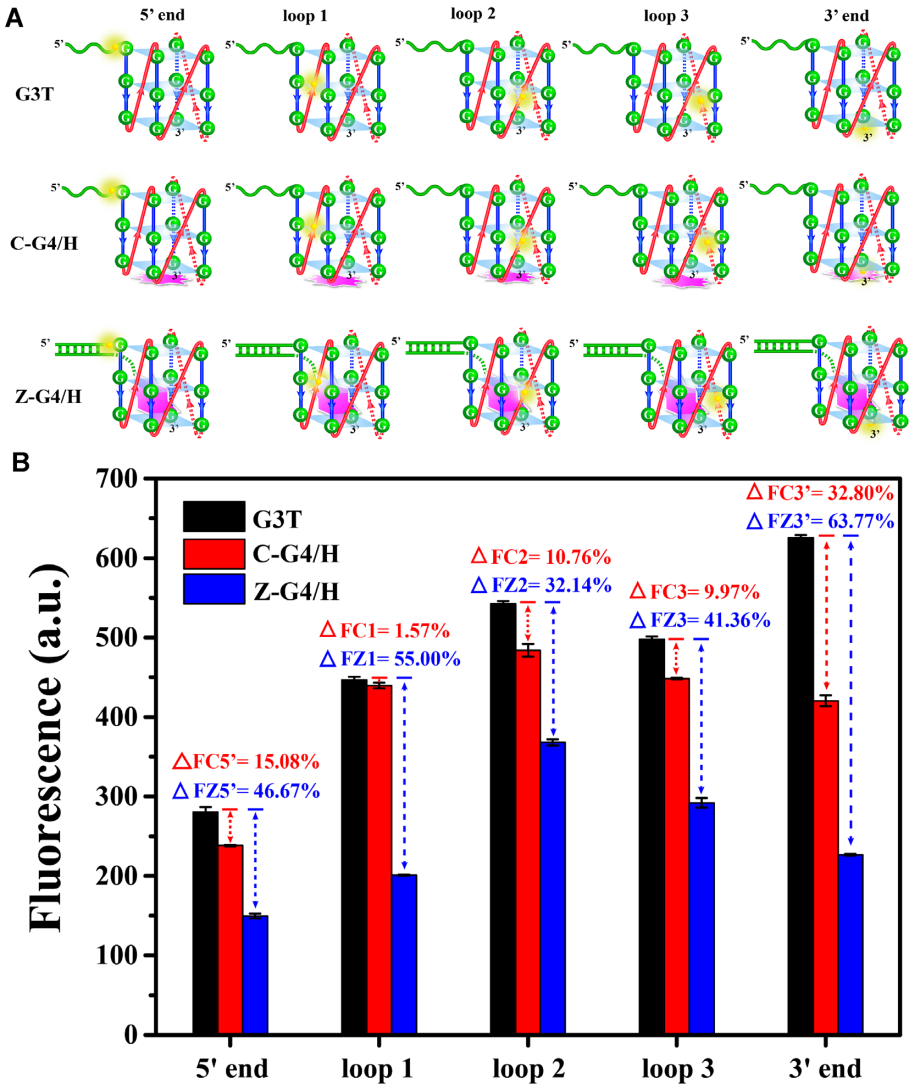

Figure 4. (**A**) Schematic representations of variant fluorescence labeling structures of G3T, C-G4/H and Z-G4/H. (**B**) Fluorescence value (excitation at 485 nm) of C-G4/H and Z-G4/H containing a FAM fluorophore at the 5'end, loop1, loop2, loop3 and 3'end, respectively. Error bars represent standard deviations of three independent experiments. ΔF represents the proportion of the fluorescence quenching.

Peroxidation behavior of the Z-G4/H

The catalytic activity of the DNAzymes displayed a linear kinetic behavior as a function of H_2O_2 concentration, revealing that the hemin-activation step for the compound I generation was the rate-determining step in the catalytic cycle (Figure 1B) (2,28). Hence, to elucidate the exact mechanism which confers enhanced catalytic activity on Z-G4/Hs, the effect of the addition of H_2O_2 on the electronic absorption spectra of DNAzymes was then investigated via UV-vis spectroscopy. Following the addition of H_2O_2, all DNAzymes displayed a hypochromicity of the Soret band at 402 nm (Figure 5A), and the decay rates of the Soret band for Z-G4/Hs were substantially faster than that of C-G4/Hs. Moreover, the dA-modified Z-G4A/H exhibited a more rapid rate than that without dA. The change in the UV-vis absorption of DNAzymes was also monitored to elucidate the intermediates of the DNAzymes further. Prior to the addition of H_2O_2, the absorption peaks of all DNAzymes gradually disappeared over 4 minutes at 480–540 and 620–650 nm, while gradually rising at 540–620 and 650–700 nm (Supplementary Figure S6), characteristic of Fe(III) intermediates formation (3). As shown in Figure 5B and 5C, faster instant disappearance time-dependent absorption peak change at E band (∼500 nm) and D band (∼625 nm) of Z-G4/Hs within the 30 s of the reaction starting, indicating the rapid formation of compound I-like intermediate in the reaction process of the Z-G4/Hs (2). These results confirmed that PECA could promote the prototropic cleavage of H_2O_2 and the formation of compound I-like intermediate, especially the dA-modification assembly one, which contributed to the enhancement of catalytic activity.

Influence of environmental conditions on Z-G4/H

The activity of DNAzymes is susceptible to environmental influence, such as H_2O_2, K^+, pH, temperature and so on. Here, catalytic kinetics experiments were performed

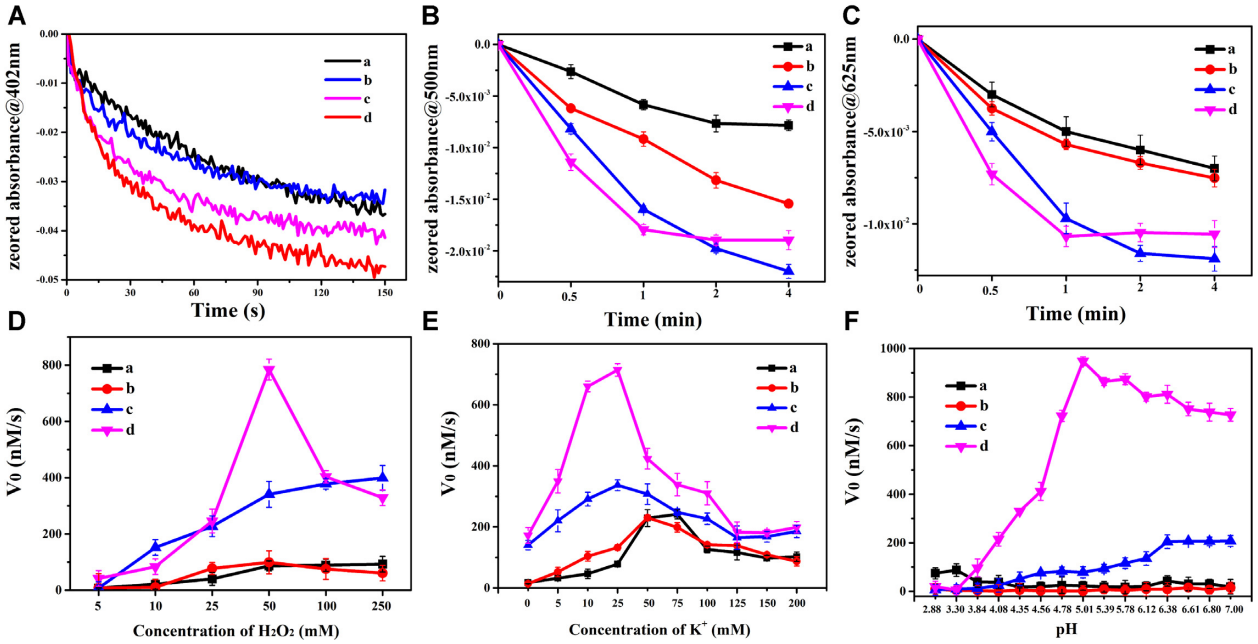

Figure 5. (**A**) Decay kinetics of (a) C-G4/H, (b) C-G4A/H, (c) Z-G4/H, (d) Z-G4A/H at 402 nm in the presence of H_2O_2 (2 mM). Change in time-dependent absorption peak in the visible region to probe the formation of the compound I-like intermediate in the reaction of DNAzymes with H_2O_2 (2 mM) at 500 nm (**B**) and 625 nm (**C**), respectively. DNAzyme activity of the four DNAzymes as a function of H_2O_2 substrate concentration (**D**), K^+ concentration (**E**) and pH (**F**), respectively. Error bars represent the standard deviations of three independent experiments.

to evaluate the optimal conditions and gain additional mechanistic insights (Supplementary Figures S7–S11). As the initiator and accelerator of the catalytic reaction, insufficient or excessive H_2O_2 leads to poor reaction kinetics (15). We observed that the initial reaction rate V_0 increased with increasing H_2O_2 concentration, and that of Z-G4/Hs were faster than C-G4/Hs, confirming the accelerated prototropic cleavage of H_2O_2 in Z-G4/Hs contributing to the exceptional catalytic capacity (Figure 5D). In addition, the maximum value of V_0 was obtained in Z-G4A/H, illustrating the intensive cleavage catalysis manner of the HRP residue-mimic PECA. Moreover, we found that excess H_2O_2 destroyed the catalyst with decreased signal, especially in the Z-G4A/H, indicating that more oxidizing agents were generated from the peroxidation reaction, leading to polynucleotide degradation. Hence, we suspected that the PECA strategy of Z-G4A/H was a more tight assembly that underwent high-density and close-range oxidative destruction during the peroxidation process.

K^+ plays a significant role in stabilizing DNAzyme for the function of G4 topology folding. As displayed in Figure 5E, the optimal K^+ concentration of Z-G4/Hs (25 mM) was less than C-G4/Hs, indicating the former required fewer K^+ than the latter. Interestingly, in contrast to the C-G4/H that requires additional ions for activity, Z-G4/Hs could even undergo catalysis without supplementary metal salts (Supplementary Figure S8). This finding perhaps was a starting point for developing DNAzyme peroxidases not readily vulnerable to complex surroundings. Furthermore, the stability of Z-G4/Hs was evaluated under different temperatures and complex surroundings. As shown in Supplementary Figure S9, the catalytic ability of Z-G4/Hs increased with increasing temperatures and achieved high-efficiency catalytic even at 95°C. On the contrary, the catalytic ability of HRP is severely affected and inactivated over 60°C, showing higher thermal stability of Z-G4/Hs than HRP. The activity of Z-G4/Hs under serum dilution surroundings also confirmed the stability and exceptional catalytic capacity of Z-G4/Hs than C-G4/Hs (Supplementary Figure S10). These findings illustrated the stability of Z-G4/Hs, resolving several contentious issues regarding DNAzyme peroxidation catalysis and making it a powerful catalytic tool to mimic protease for biomedical applications under harsh and complex environmental conditions.

Some reports suggested that dA modification of G4 DNAzymes mimics an ionizable histidine residue at the distal position of a protein peroxidase, acting as a general acid-base catalyst with a typical pH-dependent rate profile (2,30,31). This finding prompted us to evaluate the influence of pH on the catalytic efficiency of the Z-G4/Hs. As displayed in Figure 5F, the pH-rate profile of Z-G4A/H in Britton-Robinson buffer distinctly increased during pHs of approximately 3.30 to 5.01, providing evidence that the deprotonated dA (pKa value of ATP·H+/ATP being 4.2 (24)) participates in the catalysis of the peroxidation reaction. In comparison, the three other DNAzymes displayed a rate profile without association with adenine or that was feebly pH-dependent. The marked differences in pH-rate profiles between the different DNAzymes suggested that the dA-modification as the endogenous active species mimic the role of amino-acid residue in protease acting as a general acid-base catalyst and then brings about the substantial catalytic capability enhancement of Z-G4A/H. These results were consistent with our hypothesis that the dA nucleobase

supplement act as an effective distal ligand of hemin to form a more HRP-like aggregation of Z-G4A/H.

Practical applications of Z-G4/Hs in biological analysis

Understanding intracellular biomolecules interaction (e.g.,nanoscale colocation or proximity) is significant for comprehending gene expression, protein-protein interactions, cellular proliferation, and so on (40,41). However, there is still a lack of a convenient and sensitive method to monitor such a process. Proximity-induced strategies have been reported as an efficient technique to achieve biomolecular detection relying on simultaneous recognition of a pair of probes (42). Herein, we proposed a universal and sensitive approach based on PECA design to investigate the intracellular biomolecules interaction, such as gene rearrangement and protein-protein interaction. In this method, the Z-G4A/H was a useful dual-function tool for proximity recognition and catalysis. As a comparison, we employed classical split G4/hemin DNAzyme with 4:8 mode as a control group to detection the targets, which have been proved to be an optimal split mode for G4 DNAzyme-based biological detection (43-45).

The BCR/ABLp210 fusion gene is a classic biomarker of chronic myeloid leukemia, which is meaningful for for diagnosing and classifying leukemia (46). We chose e14a2 isoforms as a model analyte to elaborate on the universal and sensitive PECA strategy. As depicted in Figure 6A, a pair of probes recognize the BCRe14 domain and ABL domain via recognition sequence, respectively, and then G4 and DGH proximity assembly to an activated DNAzyme (Z-G4A/H) for catalysis (**I**). In the presence of the target gene, the absorbance spectrum (Figure 6B) and kinetics curve (Figure 6C) signal of Z-G4A/H both increased and were highest compared with split C-G4/H design (**II**), demonstrating the feasibility of the PECA strategy. Moreover, under optimal experimental conditions, the analytical properties of this strategy exhibited a good linear relationship between the absorbance signal and BCR-ABL target gene concentration over the range 0.5 nM to 100 nM, with a limit of detection (LOD) of 0.22 nM (Fig 6D), approximately 50-fold more sensitive than that of the split C-G4/H system (LOD = 11.89 nM) (Figure 6E). These results verify the clear potential of the Z-G4/H as a sensitive detection tool for biological analysis applications.

The PECA strategy was also used for imaging HER2 dimerization. The expression levels and dimerization of HER2 are considered superior markers for the diagnosis and targeted drug therapy of breast cancer (47). For instance, Trastuzumab is more effective on high levels of HER2 homodimer than other oligomerization statuses (48). As shown in Figure 7A, a pair of Z-G4A/H proximity probes (HER2-apt-G4 and HER2-DGH) were used for HER2 homodimer analysis. Where two probes are proximity recognized and bound to identical HER2 homodimers via an aptamer, the local concentration increased greatly, ultimately triggering the Z-G4A/H activated catalysis. Z-G4A/H could catalyze fluorescent tyramide deposition on proteins via DNAzyme-catalytic tyramide signal amplification (TSA) (49). Consequently, we observed a bright fluorescence signal on the surface of SKBR-3 cells (high expression of HER2 homodimers (50)), achieving sensitive imaging detection of HER2 homodimers (Figure 7B). In contrast, MCF-7 and MDA-MB-231 cells did not fluoresce due to the low expression levels of HER2 homodimers. Additionally, complete (HER2-apt-G4/hemin) and split C-G4/H system (HER2-apt-sg4 + HER2-apt-sg8/hemin) catalysis were also conducted to detect HER2 dimer protein, respectively. However, no obvious fluorescent signals were observed on the HER2 homodimer-positive SKBR-3 cell surface in our given detection system (Supplementary Figure S12). There was a weak fluorescent signal in the HER2-apt-DGH probe group for SKBR3 cell for that the single HER2-apt-DGH could catalyze a very weak tyramine-fluorescent deposited on breast cancer cells surface. These results from fluorescence imaging were further confirmed by flow cytometry, verifying the feasibility and specificity of the PECA strategy for in situ imaging of protein expression or interaction on the cell surface (Figure 7C). Hence, we developed a universal strategy with sensitive visual and imaging detection capability, which has broad practical application in clinical diagnostics and bioanalytical. Furthermore, it is also a profound potential tool for the investigation of the gene or protein expression, protein-protein interaction and so on.

DISCUSSION

The relatively insufficient catalytic ability of classical G4/hemin may be because of its simpler structure, more fragile ion-dependent folding and π-π stacking than protease. Hence, we proposed a PECA strategy to form a more HRP-like mimic, which is conceptually analogous to the tight coupling of cofactor and apoenzyme of protease. Consequently, the detailed investigations of catalytic efficiency and mechanism verified the higher activity, more rapid catalytic rate and high environmental tolerance of the Z-G4/H than C-G4/H.

Firstly, the catalytic performance of the Z-G4/H was demonstrated superior to that of C-G4/H, especially the dA modification Z-G4A/H. Based on results, we put forward several reasons: (i) More DNAzyme molecules were obtained in the Z-G4/H catalytic system of the same amount of G4 and hemin molecules due to the high solubility of DGH and the PECA design. (ii) The PECA design narrows the distance between the hemin cofactor and the apoenzyme-mimic G4 structure to form a tighter DNAzyme, more conducive to electron transfer and structural stability. (iii) Certain nucleotides (adenine or cytosine) act as ligand supplements of Z-G4/H to mimic protein residues' function and further assemble more HRP-like mimics boosting catalytic activity. Instead, dT hadn't had such a similar promoting effect. It is also worth mentioning that a nearly 3.7-fold catalytic activity increase of Z-G4A/H was observed than the previously reported intramolecular nucleobases modified G4 DNAzymes, illustrating the adenine modification in a more suitable position of the tight catalytic active center brings enhancement under the PECA strategy. Moreover, there is no overlapping effect when nucleobases are both modified on G4s and DGH, probably due to the finiteness of spatial location in the active site.

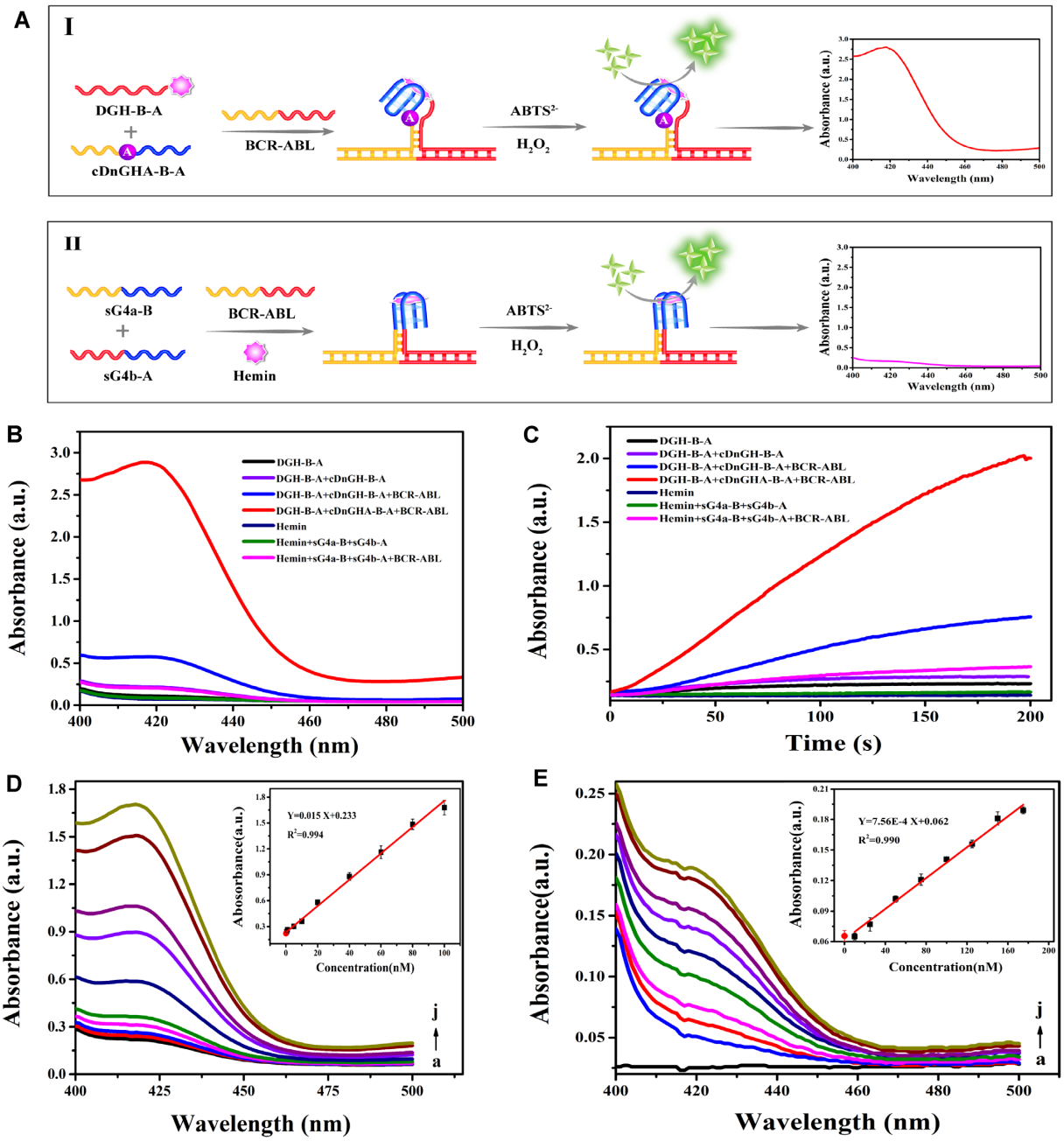

Figure 6. Schematic representation of (**A**) split C-G4/H and Z-G4A/H system for the sensitive detection of the BCR-ABL fusion gene rearrangement. Absorbance spectra (**B**) and kinetic curves (**C**) of the Z-G4A/H catalytic system for the detection of the BCR-ABL fusion gene with 2 mM $ABTS^{2-}$ and 50 mM H_2O_2. Absorbance spectra and calibration curves of (**D**) the Z-G4A/H catalytic system (100 nM DGH_5 probe) responding to 0, 0.5, 1, 5, 10, 20, 40, 60, 80 and 100 nM of the BCR-ABL fusion gene (from a to j) and (**E**) the split C-G4/H catalytic system responding to 0, 10, 25, 50, 75, 100, 125,1 50, 175 and 200 nM of the BCR-ABL fusion gene (from a to j), respectively. Error bars represent the standard deviation of three independent experiments.

Secondly, the peroxidative behavior experiments displayed that the initial reaction rate of the H_2O_2 decay in Z-G4/Hs was faster than C-G4/Hs, confirming the accelerated prototropic cleavage of H_2O_2 and electron transfer in Z-G4/Hs. Besides, the catalytic results of different concentrations of H_2O_2 indicated that Z-G4/Hs underwent a high-density and close-range oxidative destruction during the peroxidation process. Furthermore, the catalytic activity at various K^+ concentrations, temperature and complex surroundings confirmed a robust Z-G4/Hs catalytic system with lower environmental dependency and thermostability. The catalytic dynamic behavior of pH-values also indicated that Z-G4/Hs present pH-dependent catalysis typical of HRP histidine. These results demonstrated that the PECA design of the DNAzyme displayed excellent HRP-like oxidation activity, providing the one ideal alternative prototype G4/hemin DNAzyme. Nevertheless, the efforts require additional elucidation of the precise chemical group mech-

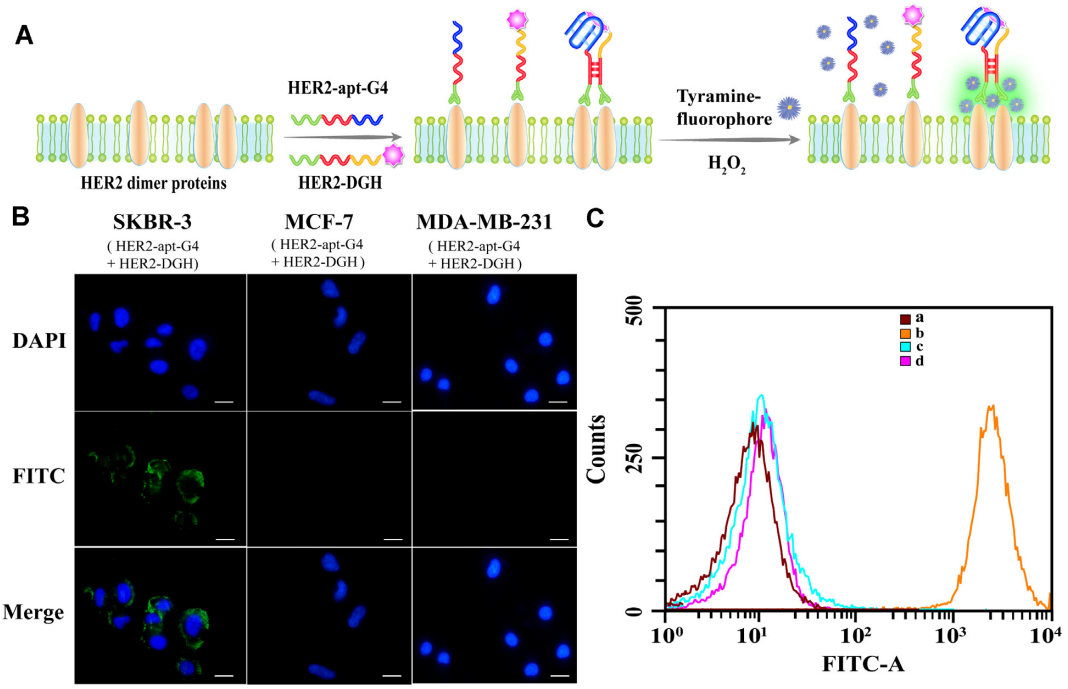

Figure 7. (**A**) Schematic representation of Z-G4A/H DNAzyme catalyzes the substrate tyramine-fluorophore for the sensitive detection of HER2 dimerization on the surface of breast cancer cells. (**B**) Fluorescence imaging of HER2 dimerization on the surface of SKBR-3, MCF-7 and MDA-MB-231 cells using the Z-G4A/H catalytic system. Scale bar: 25 μm. (**C**) Flow cytometric analysis of HER2 dimerization on the surface of (a) blank, (b) SKBR-3, (c) MCF-7 and (d) MDA-MB-231 cells using the Z-G4A/H catalytic system.

anism and position of nucleobase groups in protein-mimic catalytic active sites.

Finally, according to the exceptional capacity of Z-G4A/H, we developed a universal strategy based on PECA design realizing sensitive visual detection of the BCR-ABL fusion gene rearrangement and successfully imaging HER2 dimerization on cell surfaces, verifying the bioanalytical application potential of the strategy for detecting intramolecular interaction, including gene rearrangement, protein-protein interaction and so on. Moreover, it is also a solid basis for future research programs in G4/hemin-based biotechnology and a profound inspiration for detailed understanding and elucidation of protease mimicry establishment.

DATA AVAILABILITY

The data supporting the findings of this study are available within the paper and its Supplementary Information, and additional data are available from the corresponding author on reasonable request.

SUPPLEMENTARY DATA

Supplementary Data are available at NAR Online.

FUNDING

National Natural Science Foundation of China [81873972, 81873980, 81902164]; Natural Science Foundation of Chongqing [cstc2019jcyj-msxmX0179]; Chongqing Science Fund for Distinguished Young Scholars [cstc2019jcyjjqX0028]; Foundation for Innovative Research Groups of Chongqing Higher Education Institutions [CXQT20013]; Chongqing Medical University Graduate Talent Training Program [BJRC201908]. Funding for open access charge: National Natural Science Foundation of China [81873972].

Conflict of interest statement. None declared.

REFERENCES

1. Oscar,M., Anne,B., Jean-Baptiste,Boulé, Brosh,R.M. and Jean-Louis,M. (2016) G-quadruplexes and helicases. *Nucle Acids Res.*, **44**, 1989–2006.
2. Travascio,P., Sen,D. and Bennet,A.J. (2006) DNA and RNA enzymes with peroxidase activity-an investigation into the mechanism of action. *Can. J. Chem.*, **84**, 613–619.
3. Yang,X., Fang,C., Mei,H., Chang,T., Cao,Z. and Shangguan,D. (2011) Characterization of G-quadruplex/hemin peroxidase: substrate specificity and inactivation kinetics. *Chemistry*, **17**, 14475–14484.
4. Poon,C.H., Methot,S.P., Morabi-Pazooki,W., Pio,F., Bennet,A.J. and Sen,D. (2011) Guanine-rich RNAs and DNAs that bind heme robustly catalyze oxygen transfer reactions. *J. Am. Chem. Soc.*, **133**, 1877–1884.
5. Hiroshi,A. and Belcher,A.M. (2018) DNA origami and G-quadruplex hybrid complexes induce size control of single-walled carbon nanotubes via biological activation. *ACS Nano*, **12**, 7986–7995.
6. Peng,H., Newbigging,A.M., Wang,Z., Tao,J., Deng,W. and Le,X.C. (2018) DNAzyme-mediated assays for amplified detection of nucleic acids and proteins. *Anal.Chem.*, **90**, 190–207.
7. Bingling,L., Ellington,A.D. and Xi,C. (2011) Rational, modular adaptation of enzyme-free DNA circuits to multiple detection methods. *Nucleic Acids Res.*, **39**, e110.

8. Huang,R., He,L., Xia,Y., Xu,H., Liu,C., Xie,H., Wang,S., Peng,L., Liu,Y., Liu,Y. *et al.* (2019) A sensitive aptasensor based on a hemin/G-quadruplex-assisted signal amplification strategy for electrochemical detection of gastric cancer exosomes. *Small*, **15**, e1900735.
9. Travascio,P., Li,Y. and Sen,D. (1998) DNA-enhanced peroxidase activity of a DNA-aptamer-hemin complex. *Chem. Biol.*, **5**, 505–517.
10. Sen,D. and Poon,L.C.H. (2011) RNA and DNA complexes with hemin [Fe(III) heme] are efficient peroxidases and peroxygenases: how do they do it and what does it mean? *Crit. Rev. Biochem. Mol.*, **46**, 478–492.
11. Shumayrikh,N., Huang,Y.C. and Sen,D. (2015) Heme activation by DNA: isoguanine pentaplexes, but not quadruplexes, bind heme and enhance its oxidative activity. *Nucleic Acids Res.*, **43**, 4191–4201.
12. Stefan,L., Denat,F. and Monchaud,D. (2011) Deciphering the DNAzyme activity of multimeric quadruplexes: insights into their actual role in the telomerase activity evaluation assay. *J. Am. Chem. Soc.*, **133**, 20405–20415.
13. Einarson,O.J. and Sen,D. (2017) Self-biotinylation of DNA G-quadruplexes via intrinsic peroxidase activity. *Nucleic Acids Res.*, **45**, 9813–9822.
14. Ai,T., Yang,Q., Lv,Y., Huang,Y., Li,Y. and Geng,J. (2018) Insight into how telomeric G-quadruplexes enhance the peroxidase activity of cellular hemin. *Chem. - .Asian. J.*, **13**, 1805–1810.
15. Mingpan,C., Yu,C., Jingya,H., Guoqing,J. and Jean-Louis,M. (2018) Loop permutation affects the topology and stability of G-quadruplexes. *Nucleic Acids Res.*, **46**, 9264–9275.
16. Agrawal,P., Lin,C., Mathad,R.I., Carver,M. and Yang,D. (2014) The major G-quadruplex formed in the human BCL-2 proximal promoter adopts a parallel structure with a 13-nt loop in K^+ solution. *J. Am. Chem. Soc.*, **136**, 1750–1753.
17. Punt,Philip M. and Clever,G.H. (2019) Imidazole-modified G-quadruplex DNA as metal-triggered peroxidase. *Chem. Sci.*, **10**, 2513–2518.
18. Travascio,P., Witting,P.K., Mauk,A.G. and Sen,D. (2001) The peroxidase activity of a hemin-DNA oligonucleotide complex: free radical damage to specific guanine bases of the DNA. *J. Am. Chem. Soc.*, **123**, 1337–1348.
19. Chen,J., Cheng,M., Salgado,G.F., Stadlbauer,P., Zhang,X., Amrane,S., Guédin,A., He,F., Šponer,J., Ju,H. *et al.* (2021) The beginning and the end: flanking nucleotides induce a parallel G-quadruplex topology. *Nucleic Acids Res.*, **49**, 9548–9559.
20. Zhang,K., Lv,S., Lin,Z. and Tang,D. (2017) Cds:mn quantum dot-functionalized g-c3n4 nanohybrids as signal-generation tags for photoelectrochemical immunoassay of prostate specific antigen coupling dnazyme concatamer with enzymatic biocatalytic precipitation. *Biosens. Bioelectron.*, **95**, 34–40.
21. Ravichandran,S., Razzaq,M., Parveen,N., Ghosh,A. and Kim,K.K. (2021) The effect of hairpin loop on the structure and gene expression activity of the long-loop G-quadruplex. *Nucleic Acids Res.*, **49**, 10689–10706.
22. Zhang,K., Lv,S., Lin,Z., Li,M. and Tang,D. (2018) Bio-bar-code-based photoelectrochemical immunoassay for sensitive detection of prostate-specific antigen using rolling circle amplification and enzymatic biocatalytic precipitation. *Biosens. Bioelectron.*, **101**, 159–166.
23. Wang,Q., Xu,N., Lei,J. and Ju,H. (2014) Regulative peroxidase activity of DNA-linked hemin by graphene oxide for fluorescence DNA sensing. *Chem. Commun.*, **50**, 6714–6717.
24. Wang,Q., Xu,N., Gui,Z., Lei,J., Ju,H. and Yan,F. (2014) Catalytic activity of a dual-hemin labelled oligonucleotide: conformational dependence and fluorescent DNA sensing. *Chem. Commun.*, **50**, 15362–15365.
25. Li,J., Yuan,T., Yang,T., Xu,L., Zhang,L., Huang,L., Cheng,W. and Ding,S.J. (2018) DNA-grafted hemin with preferable catalytic properties than G-quadruplex/hemin for fluorescent miRNA biosensing. *Sens. Actuators B: Chem.*, **271**, 239–246.
26. Li,J., Xiang,Y., Zhang,L., Huang,L., Teng,J. and Ding,S. (2019) Dynamic DNA self-assembly activated hemin-mimetic enzyme system for versatile fluorescent biosensing. *Sens. Actuators B: Chem.*, **288**, 757–762.
27. Cheng,X., Liu,X., Bing,T., Cao,Z. and Shangguan,D. (2009) General peroxidase activity of G-quadruplex-hemin complexes and its application in ligand screening. *Biochem.*, **48**, 7817–7823.
28. Stefan,L., Denat,F. and Monchaud,D. (2012) Insights into how nucleotide supplements enhance the peroxidase-mimicking DNAzyme activity of the G-quadruplex/hemin system. *Nucleic Acids Res.*, **40**, 8759–8772.
29. Qi,C., Zhang,N., Yan,J., Liu,X., Bing,T. and Mei,H. (2014) Activity enhancement of G-quadruplex/hemin DNAzyme by spermine. *RSC Adv.*, **4**, 1441–1448.
30. Li,W., Li,Y., Liu,Z., Lin,B., Yi,H., Xu,F., Nie,Z. and Yao,S. (2016) Insight into G-quadruplex-hemin DNAzyme/RNAzyme: adjacent adenine as the intramolecular species for remarkable enhancement of enzymatic activity. *Nucleic Acids Res.*, **44**, 7373–7384.
31. Chen,J., Zhang,Y., Cheng,M., Guo,Y., Sponer,J., Ju,H.X. and Zhou,J. (2018) How proximal nucleobases regulate the catalytic activity of G-quadruplex/hemin DNAzymes. *ACS Catal.*, **8**, 11352–11361.
32. Chang,T., Gong,H., Ding,P., Liu,X., Li,W. and Bing,T. (2016) Activity enhancement of G-quadruplex/hemin DNAzyme by flanking d(CCC). *Chem. - Eur. J.*, **22**, 4015–4021.
33. Chen,J., Guo,Y., Zhou,J. and Ju,H. (2017) The effect of adenine repeats on G-quadruplex/hemin peroxidase mimicking DNAzyme activity. *Chem. - Eur. J.*, **23**, 4210–4215.
34. Nakayama,S., Wang,J. and Sintim,H.O. (2011) DNA-based peroxidation catalyst-what is the exact role of topology on catalysis and is there a special binding site for catalysis? *Chem. - Eur. J.*, **17**, 5691–5698.
35. Evans,S.E., Mendez,M.A., Turner,K.B., Keating,L.R., Grimes,R.T., Melchoir,S. and Szalai,V.A. (2007) End-stacking of copper cationic porphyrins on parallel-stranded guanine quadruplexes. *J. Biol. Inorg. Chem.*, **12**, 1235–1249.
36. Nakayama,S. and Sintim,H.O. (2009) Colorimetric split G-quadruplex probes for nucleic acid sensing: improving reconstituted DNAzyme's catalytic efficiency via probe remodeling. *J. Am. Chem. Soc.*, **131**, 10320–10333.
37. Li,D., Cheng,W., Li,Y., Xu,Y., Li,X., Yin,Y., Ju,H. and Ding,S. (2016) Catalytic Hairpin Assembly Actuated DNA Nanotweezer for Logic Gate Building and Sensitive Enzyme-Free Biosensing of MicroRNAs. *Anal. Chem.*, **88**, 7500–7506.
38. Pavlov,V., Xiao,Y., Gill,R., Dishon,A., Kotler,M. and Willner,I. (2004) Amplified chemiluminescence surface detection of DNA and telomerase activity using catalytic nucleic acid labels. *Anal. Chem.*, **76**, 2152–2156.
39. Fan,D., Zhu,X., Dong,S. and Wang,E. (2017) Tyramine hydrochloride based label-free system for operating various DNA logic gates and a DNA caliper for base number measurements. *Chem. Phys. Chem.*, **18**, 1767–1772.
40. You,M., Zhu,G., Chen,T., Donovan,M.J. and Tan,W. (2015) Programmable and multiparameter DNA-based logic platform for cancer recognition and targeted therapy. *J. Am. Chem. Soc.*, **137**, 667–674.
41. Pellejero,L.B., Mahdifar,M., Ercolani,G., Watson,J., Brown,T. Jr and Ricci,F. (2020) Using antibodies to control DNA-templated chemical reactions. *Nat. Chem.*, **11**, 6242.
42. Xue,J., Chen,F., Su,L., Cao,X., Bai,M., Zhao,Y., Fan,C. and Zhao,Y. (2021) Pairwise proximity-differentiated visualization of single-cell DNA epigenetic marks. *Angew. Chem. Int. Ed.*, **60**, 3428–3432.
43. Zhu,J., Zhang,L., Dong,S. and Wang,E. (2015) How to split a G-quadruplex for DNA detection: new insight into the formation of DNA split G-quadruplex. *Chem. Sci.*, **6**, 4822–4827.
44. Shimron,S., Wang,F., Orbach,R. and Willner,I. (2012) Amplified detection of DNA through the enzyme-free autonomous assembly of hemin/G-quadruplex DNAzyme nanowires. *Anal. Chem.*, **84**, 1042–1048.
45. Lv,M., Guo,Y., Ren,J. and Wang,E. (2019) Exploration of intramolecular split G-quadruplex and its analytical applications. *Nucleic Acids Res.*, **47**, 9502–9510.
46. de Klein,A., van Agthoven,T., Groffen,C., Heisterkamp,N., Groffen,J. and Grosveld,G. (1986) Molecular analysis of both translocation products of a Philadelphia-Positive CML patient. *Nucleic Acids Res.*, **14**, 7071–7082.
47. Slamon,D.J., Clark,G.M., Wong,S.G., Levin,W.J., Ullrich,A. and McGuire,W.L. (1987) Human breast cancer: correlation of relapse and survival with amplification of the HER-2/neu oncogene. *Science*, **235**, 177–182.
48. Ghosh,R., Narasanna,A., Wang,S.E., Liu,S., Chakrabarty,A., Balko,J.M., González-Angulo,A.M., Mills,G.B., Penuel,E.,

Winslow,J. *et al.* (2011) Trastuzumab has preferential activity against breast cancers driven by HER2 homodimers. *Cancer Res.*, **71**, 1871–1882.
49. Yuan,L., Xu,L. and Liu,S. (2012) Integrated tyramide and polymerization-assisted signal amplification for a highly-sensitive immunoassay. *Anal. Chem.*, **84**, 10737–10744.
50. Rusnak,D.W., Alligood,K.J., Mullin,R.J., Spehar,G.M., Arenas-Elliott,C., Martin,A.M., Degenhardt,Y., Rudolph,S.K., Haws,T.F. Jr, Hudson-Curtis,B.L. *et al.* (2007) Assessment of epidermal growth factor receptor (EGFR, ErbB1) and HER2 (ErbB2) protein expression levels and response to lapatinib (Tykerb, GW572016) in an expanded panel of human normal and tumour cell lines. *Cell Proliferat.*, **40**, 580–594.